Chemistry
A European
Journal

Chemistry
Europe
European Chemical
Societies Publishing

**Title:** Fabrication of Pd/Mg2P2O7 via a Struvite-template Way from Wastewater and Application as Chemoselective Catalyst in Hydrogenation of Nitroarenes

**Authors:** Peng Zhang, Shaonan Xu, Yan Wang, Wei Zhang, Wenqing Li, Cundi Wei, Peiping Zhang, and Shiding Miao

**To be cited as:** *Chem. Eur. J.* 10.1002/chem.202100684

**Link to VoR:** https://doi.org/10.1002/chem.202100684

WILEY-VCH

WILEY-VCH

# Fabrication of $Pd/Mg_2P_2O_7$ via a Struvite-template Way from Wastewater and Application as Chemoselective Catalyst in Hydrogenation of Nitroarenes

Dr. Peng Zhang,[a] Shaonan Xu,*[a] Dr. Yan Wang,[b] Dr. Wei Zhang,[b] Wenqing Li,[c] Prof. Cundi Wei,[a] Prof. Peiping Zhang,[a] and Prof. Shiding Miao*[a]

[a] *Dr. P. Zhang, S. N. Xu, Prof. C. D. Wei, Prof. P. P. Zhang, Prof. S. D. Miao*
*Key Laboratory of Automobile Materials of Ministry of Education, School of Materials Science and Engineering, Solid Waste Recycling Engineering Research Center of Jilin Province, Open Research Laboratory for Physicochemical Testing Methods of Functional Minerals-Ministry of Natural Resources, Jilin University, Changchun, 130022, China; E-mail: xsn@jlu.edu.cn (S. Xu) and miaosd@iccas.ac.cn (S. Miao)*
[b] *Dr. Y. Wang, Dr. W. Zhang*
*State Key Laboratory of Mineral Processing, BGRIMM Technology Group, No. 188, South 4th Ring Road West, Beijing, China*
[c] *W. Q. Li*
*Key Laboratory of Mineral Resources Evaluation in Northeast Asia, Ministry of Natural Resources, Changchun 130061, China*

**Keywords:** Struvite synthesis; Mesoporous magnesium pyrophosphate; Heterogeneous catalyst; Chemoselective catalysis; Nitroarenes hydrogenation

**Abstract:** A highly efficient heterogeneous catalyst $Pd/Mg_2P_2O_7$ was fabricated by combining palladium nanoparticles (Pd NPs) and mesoporous $Mg_2P_2O_7$ fibers/rods. The $Mg_2P_2O_7$ fibers with ultra high specific surface area were prepared from struvite as templates which were synthesized from waste water consisting of N- and P-containing pollutants. This strategy provided a novel pathway in developing advanced catalysts from eutrophication polluted water. The composite $Pd/Mg_2P_2O_7$ showed brilliant performance in selective hydrogenation of nitro-aromatics to get anilines. As an example of nitrobenzene hydrogenation, the conversion and selectivity to aniline were found to reach almost 100% at temperature of T=90 ℃ and under pressure of $P_{H2}$=2.0 MPa. The superior performance was found to originate from Pd NPs which were boosted by electron transfer afforded by the nano-fibers $Mg_2P_2O_7$ supports. The favorable adsorption of withdrawing groups ($-NO_2$) was realized by synergistic effects between Pd and oxygen vacancies provided by pyrolysis of struvite. The catalyst remained stably after cycles of reuse with little degradation in catalysis.

## 1. Introduction

Although nitrogen (N) and phosphorus (P) are essential nutrients for bio-activities [1, 2], the over enrichment with such nutrients can be an environmental concern for rivers, lakes, wetlands, streams, and reservoirs worldwide. Currently the high concentration of phosphate and ammonium was found in many lakes of east China, and the eutrophication pollution was serious [3]. To reconcile eutrophication, a good choice is to precipitate the soluble N-, P-nutrients and transform them into inorganic minerals, i.e., to mineralize such pollutants [4]. Struvite is one of the common N-, P-containing minerals with a formula of $MgNH_4PO_4 \cdot 6H_2O$, sometimes been referred to the misnomer “triple phosphate” [5]. Due to the nutritional content of P and N and low solubility in aqueous solutions, struvite was considered as an ideal slow-release food/fertilizer for animals/plants [6, 7]. Struvite can also work as functional minerals as pH-regulator [8], but there were few reports of struvite tested as catalysts.

Aromatic anilines are important chemicals for production of pharmaceuticals, dyestuffs, agrochemicals, pigments and polymers [9]. Current industrial production of aromatic anilines usually employed catalytic hydrogenation of nitroarene in the liquid phase. Nevertheless, the nitroarene often has one or more hrdrgenation group (C=C, C≡C, -OH and so on) which bring great challenges for chemoselective hydrogenation. Therefore, the preparation efficient and environmentally friendly catalysts for chemoselective hydrogenation of nitroarene are the focus of scientific research and industrial production. It has been found that using heterogeneous catalysts in selective hydrogenation of nitro-aromatic compounds, and transforming nitro into amino groups is an effective method [10, 11]. As is known, nitro is a strong electron-withdrawing group, and can be activated by electron-rich catalytic sites [12]. Noble metals would facilitate such reactions. The strong interaction between noble metals and nitro-aromatics would determine the pathway of hydrogenation [13, 14]. The support was also found to have a great influence on electron withdrawing capacity [15]. The interfacial contact

10.1002/chem.202100684

induced by strong metal-support bonds would make electrons redistributed and impart favorable environments for catalysis [16]. The catalyst support should be designed as transferring electrons and making active sites electron-rich. Phosphates have abundance of acidic sites that afford the P-based materials as electron withdrawing catalysts for many reactions [17]. The phosphate based catalysts were able to increase the surface hydrophobicity of catalyst, which can maintain high activity in polar solvent [18], and this would strengthen chemo-selectivity for hydrogenation reactions. In the past decades the mesoporous phosphates have emerged as promising materials in various fields such as in catalysis, wastewater treatment, sorption, energy storage and biomedicine [19, 20]. However, the difficulty in preparation of mesoporous phosphates lies in the high reactivity of phosphate precursors which would hydrolyze at an uncontrollable rate, and this made less possible to prepare mesoporous phosphate materials [21].

In this research the struvite nano-fibers were synthesized from simulated wastewater, and the mesoporous material, magnesium pyrophosphate ($Mg_2P_2O_7$), was successfully prepared after thermal decomposition. The state-of-art was schematically shown in Scheme 1. The fabrication details were provided in the experimental. The fibrous $Mg_2P_2O_7$ with mesoporous structure was used to support palladium (Pd) nanoparticles (NPs) to get a new type of heterogeneous catalysts, and these materials were validated to be efficient in selective hydrogenation of nitro-aromatics to amino-aromatics. The prepared struvite of fiber- or rod-shapes ($MgNH_4PO_4 \cdot 6H_2O$) were found to be decomposed and release $NH_3$ at certain temperature (~250 ℃), and to yield porous nano-fibers $Mg_2P_2O_7$ with remaining little nitrogen (N) [22]. This art provided a way of obtaining uniform mesoporous $Mg_2P_2O_7$ material which was able to be facilely loaded with Pd NPs. The N-doped materials were considered as promising supports in the heterogeneous catalysis [23]. As is known, phosphorus (P) has the same valence states as nitrogen (N) in most compounds, but the former shares a larger atomic radius and better electron-donating capacity [24]. Therefore, our prepared $Mg_2P_2O_7$ was a more metal-like electronic structure and generated more defect sites [25]. This feature was effective in activating hydrogen and selectively adsorbing electron-withdrawing functional groups on the catalyst surface.

Generally, the activation and dissociation of $H_2$ were assumed as most important steps in hydrogenation reactions. Among various metal nanoparticles, the palladium catalysts exhibited remarkable activity [26]. The Pd NPs were able to activate $H_2$ under mild conditions, and facilitated bond formation between nitro groups and the dissociated H atoms [27]. Reasons lie in the fact that Pd NPs share a large number of delocalized electrons, which provides suitable $H_2$ to interact with nitro groups [28]. Therefore, suitable choice of supports would be of great importance in getting uniform dispersed Pd NPs, to protect Pd NPs from aggregation, and to improve catalytic efficiency/selectivity. This study was focused on synthesizing struvite nano-fibers from wastewater, and a type of high specific surface area materials with mesoporous structures was obtained through pyrolysis of these nano-fibers (struvite). Through metal-support interaction, electrons of Pd NPs were transferred to mesopores support of magnesium pyrophosphate ($Mg_2P_2O_7$) for promoting the selective adsorption of nitro groups. The Lewis acidity of $Mg_2P_2O_7$ on hydrogenation path of nitroaromatic compounds and phosphorus owning to the electron-donating ability were found to regulate catalysis, and the high activity and selectivity for nitroarenes was achieved.

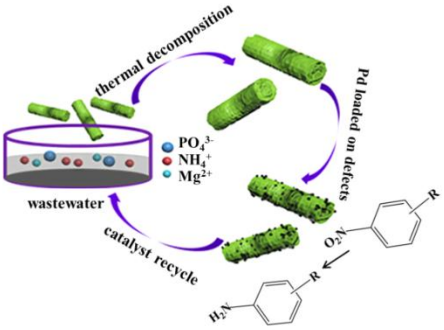

**Scheme 1** Schematic illustration of the catalyst Pd/$Mg_2P_2O_7$ nano-fibers fabricated for chemoselective hydrogenation of nitroarenes.

10.1002/chem.202100684

## 2. Results and discussion

### 2.1 Material characterizations

As shown by XRD patterns in Figure 1, the as-synthesized struvite was demonstrated to have a distinctive orthorhombic structure by indexing intensity and position of XRD reflection peaks to the database for mineral identification. The result implied the main crystalline phase was well indexed to struvite [$Mg(NH_4)PO_4\ 6H_2O$] (PDF#15-0762) with minor cattiite [$Mg_3(PO_4)_2 \cdot 22H_2O$] [29]. The same orthorhombic system $Mg_2P_2O_7$ was confirmed after pyrolysis of struvite, i.e., after release of some gaseous substances. In this research the Pd nanoparticles were synthesized according to the previous method [30], and the face-centered cubic structure of Pd (PDF#46-1043) was observed based on plans of (111), (200), and (220) as shown in the XRD pattern (Figure S1, see the supporting information, SI) [31]. When the Pd NPs were introduced into mesoporous support of $Mg_2P_2O_7$, the relative intensity of the support did not change. However, the characteristic XRD reflection of Pd NPs was not observed which indicated that the Pd NPs were homogeneously dispersed, and the particle sizes were too small to display XRD reflections in the Pd-struvite nano-fibers (Figure 1) [32].

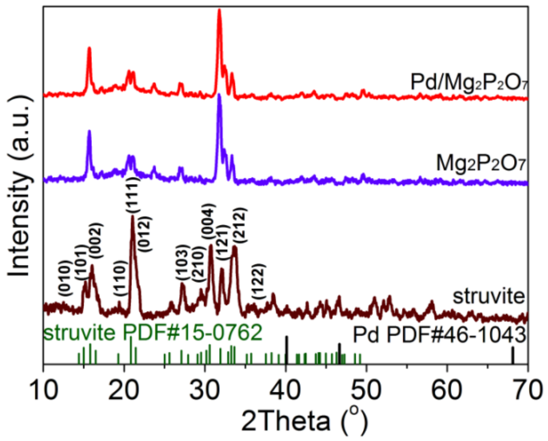

**Figure 1** XRD patterns of the as-synthesized struvite nano-fibers (struvite), thermal treated sample at 250°C ($Mg_2P_2O_7$), and the final Pd/$Mg_2P_2O_7$ after loading Pd NPs.

The field-emission SEM (FESEM) was used to characterize the micro-structure as shown in Figure 2. Nano-fibers or rods were observed to have an average length of 5-15 μm and width of 200-600 nm. No other morphologies were found in the as-synthesized struvite. This indicated this method is effective in yielding nano-fiber struvite (Figure 2a). The magnified image of struvite (Figure 2b) showed there were almost no mesoporous structures on the struvite fibers. However, there appeared numerous pores in the pyrolysis sample $Mg_2P_2O_7$, suggesting the volatile substance ($NH_3$ and $H_2O$, confirmed by TG-MS) is a key factor to generate porosity. As shown in Figure 2c, dense packing of pores was found, and these pores had a uniform sizes about 30 nm. The mesoporous fiber seemed to have rolled-up texture from layers of $Mg_2P_2O_7$. The open mouth morphology was more clearly observed as evidenced by inset in Figure 2c. The SEM of composite $Pd/Mg_2P_2O_7$ was shown in Figure 2d. It was found that the mesoporous fibers were loaded with Pd NPs everywhere. The surface of mesoporous fibers seemed rougher under SEM observation due to presence of numerous particles. In order to verify elements of the final catalyst the energy-dispersive X-ray spectroscopy (EDS) were shown in Figure 2e~f &S2, which confirmed the major elements of Mg, N, O, P and Pd that were homogeneously distributed along the struvite fiber. Although the nitrogen content was less than those of constituent elements of struvite, nitrogen was validated to be remained in the final composite as a doping element.

10.1002/chem.202100684

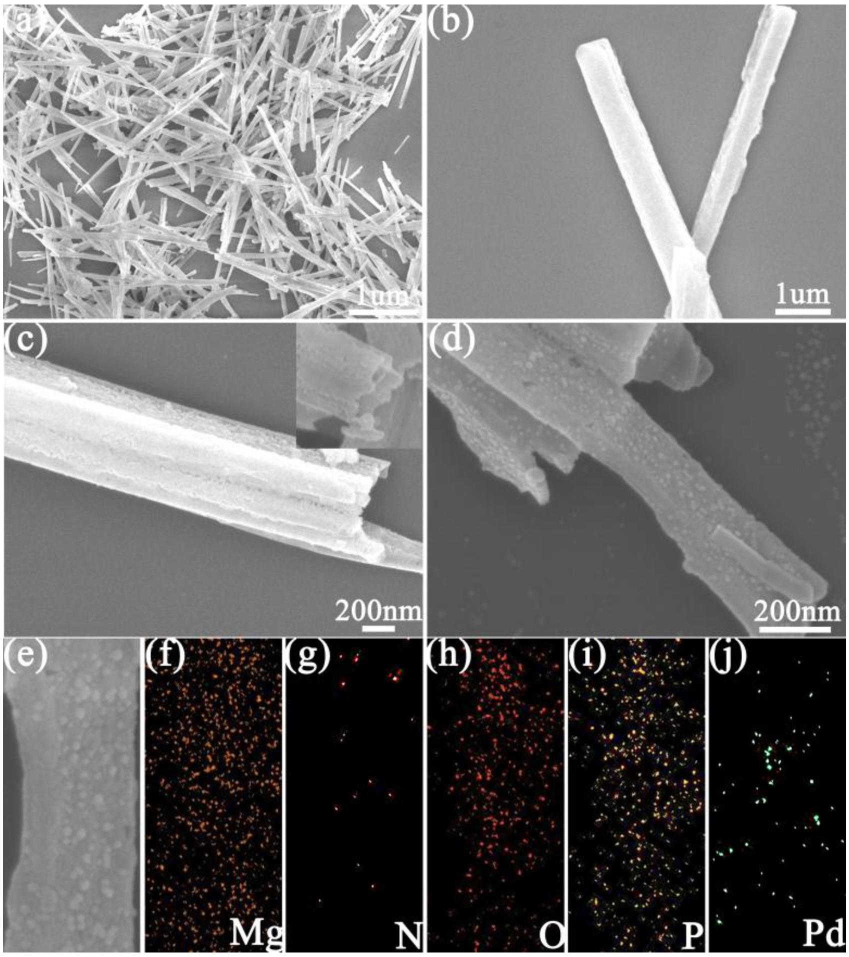

**Figure 2** (a, b) SEM image of struvite synthesized from wastewater; (c) SEM image of struvite after thermal treatment at 250 ℃ for 1 h (sample $Mg_2P_2O_7$); (d) SEM image of the sample Pd/$Mg_2P_2O_7$; (e~j) EDS elemental mapping (Mg, N, O, P, Pd) of the selected area on a single fiber of Pd/$Mg_2P_2O_7$.

The detail microstructure after struvite pyrolysis was further studied by the TEM analysis. The struvite with large, micro-sized fibrous morphology was found in Figure 3a. The mesoporous materials were obtained from the struvite at different pyrolysis rates 2 ℃/min, 4 ℃/min, 6 ℃/min and 8 ℃/min which were shown by Figure S3 in the SI. The pore-making mechanism could be explained by the fact that the volatilization rate of ammonia gas determined the mesoporous size of the support. These corresponding to the pore sizes of the support surface are 14, 30, 50 and 80 nm, respectively. To effectively prevent the loss of Pd NPs in the catalytic process and reduce its agglomeration, the support with pore size

10.1002/chem.202100684

distribution of 30 nm was finally selected. As confirmed by TEM morphology shown Figure 3b, the sample of $Mg_2P_2O_7$ was obtained after thermal treatment at 250 ℃ but still remained as fibrous shapes. The highly porous character was observed. Pores were densely arranged along the fiber, and were of uniform size about 30 nm. Insert in Figure 3b was the enlarged TEM image which displayed the d-spacing of 0.117 nm corresponding to the (111) plane of $Mg_2P_2O_7$. Therefore, the thermal treated struvite would lead to mesoporous fibers, and the fibers were constructed with crystalline $Mg_2P_2O_7$ walls. The presence of Pd NPs was confirmed by the prominent contrast between struvite substrate and black points of metallic NPs under the TEM observation (Figure 3c in the main manuscript and Figure S4 in the SI). Figure 3c and 3d indicated that the Pd NPs were highly dispersed on the surface of nano-fibers as well as loaded in mesopores. The average size of Pd NPs was evaluated to be ~10 nm in histogram profiles (Figure S5, see the SI). The high-resolution TEM of Pd NPs displayed interplanar spacing of 0.226 nm which agreed well with the (111) plane of cubic Pd [33]. The image of inset in Figure 3d indicated Pd NPs were of face-centered cubic structure. The scanning TEM (STEM) images of bright/dark field for Pd/$Mg_2P_2O_7$ were showed in the Figure 3e and 3f. It could be seen that the Pd NPs were uniformly dispersed over the inner and outer surface of the nano-fibers.

10.1002/chem.202100684

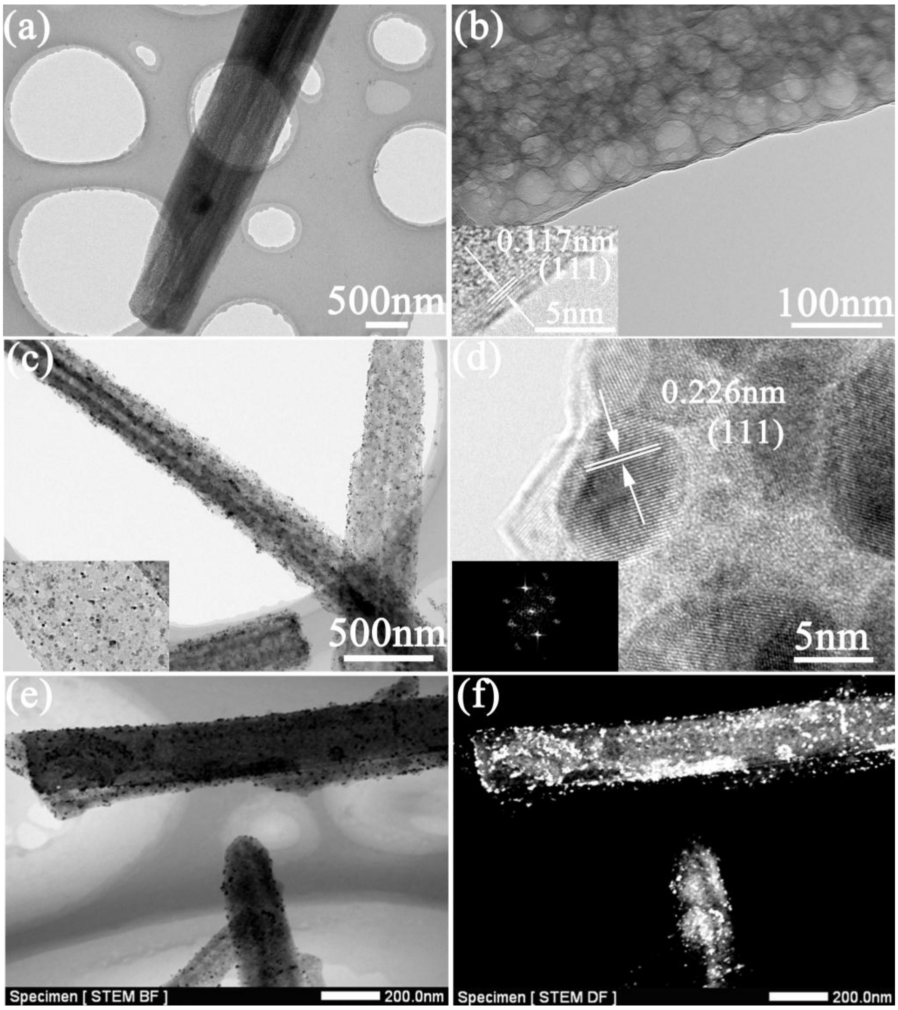

**Figure 3** (a~d) TEM images of the as-synthesized struvite (a), mesoporous fibers of $Mg_2P_2O_7$ (b), Pd/$Mg_2P_2O_7$ catalyst (c), and HRTEM images of Pd nanocrystals (d), Insert in Figure 3d is the fast Fourier transform (FFT) pattern. (e~f) STEM images of catalyst for bright (g)/dark (f) field, respectively.

To further investigate chemical states the XPS measurements were characterized on struvite and the final Pd/$Mg_2P_2O_7$. Elements of C1s, Mg1s, N1s, P2p and Pd3d bands were observed in all samples as shown by the wide-range XPS spectrum (Figure 4a). All XPS spectra were referenced to the peak 284.8 eV of C1s. The Mg 1s spectrum of Figure 4b was located at 1302.7 eV [34]. The N 1s spectrum could be decovoluted into three bands which correspond to different N species: pyridinic N (399.2 eV), pyrrolic N (400.3 eV), graphitic N (401.1 eV) [35]. By comparing nitrogen peaks of struvite with those of Pd/$Mg_2P_2O_7$, the N content was greatly reduced after pyrolysis. And the content of N was only 0.01 atomic % by ICP measurement.

In the high-resolution XPS spectrum Pd 3d (Figure 4d) of sample Pd/$Mg_2P_2O_7$, the signal of Pd NPs was composed with two doublets which were indexed to the spin-orbit couplings. The components Pd $3d_{5/2}$ (335.3 eV) and Pd $3d_{3/2}$ (339.8 eV) could be assigned to species of $Pd^0$ and $Pd^{II}O$ [36]. The higher doublet 337.1 eV and 341.4 eV was attributable to $Pd^{2+}$ which reasons might be the partial oxidation due to exposure to air. The other two peaks with lower binding energy (334.4 and 339.6 eV) were corresponded to the $Pd^0$. It was worth noting that the signal between $Pd^0$ and $Pd^{2+}$ was found to shift toward higher binding energy with respect to the neat Pd NPs. It could be explained as a result of a partial valence orbital overlapped between surface Pd atoms and the substrate of P element in struvite [24]. The Pd NPs presented electron-depleted behavior on the surface of support, which suggested the electron transfer from Pd toward the $Mg_2P_2O_7$, and this would make the surface of catalyst enriched with electron [37]. Therefore the composite was indicated to be more prone to attract nitro groups (-$NO_2$). To understand the electron transfer, the work function between Pd NPs to $Mg_2P_2O_7$ could be explained. The work function of Pd NPs is 5.24 eV and the support for $Mg_2P_2O_7$ is 5.58 eV. This caused a significant electron transfer from Pd NPs to $Mg_2P_2O_7$ [38]. This indication could be caused by the interaction of P element and Pd. The deconvolution of P 2p spectrum confirmed the P $2p_{3/2}$ and P $2p_{1/2}$ peaks. Interestingly the P 2p XPS bands in $Mg_2P_2O_7$ and Pd/$Mg_2P_2O_7$ both had three components. The highest binding energy of P 2p in $Mg_2P_2O_7$ located at 133.9 eV and 134.1 eV, respectively. They are assigned to oxidized phosphorus species which correspond to P-O-P, P-OH and P=O [39]. However, the phosphorus oxides species in the Pd/$Mg_2P_2O_7$ was weakened, which implied the presence of electron interactions between Pd NPs and element of P. The intermediate binding energy (132.7 eV in Pd/$Mg_2P_2O_7$) was attributed to bonds of Pd-P. The P 2p peaks at 131.4 eV (Pd/$Mg_2P_2O_7$) likely interacted with Pd NPs. Through the comparison of the P 2p ratio of the element state in two samples, it could be conclude that there is strong interaction between P and Pd NPs. It could also be seen that the binding energy of P 2p in the catalyst shift to smaller energy, which further confirmed the interaction between metals and support would promote electrons transfer from Pd to the support of $Mg_2P_2O_7$.

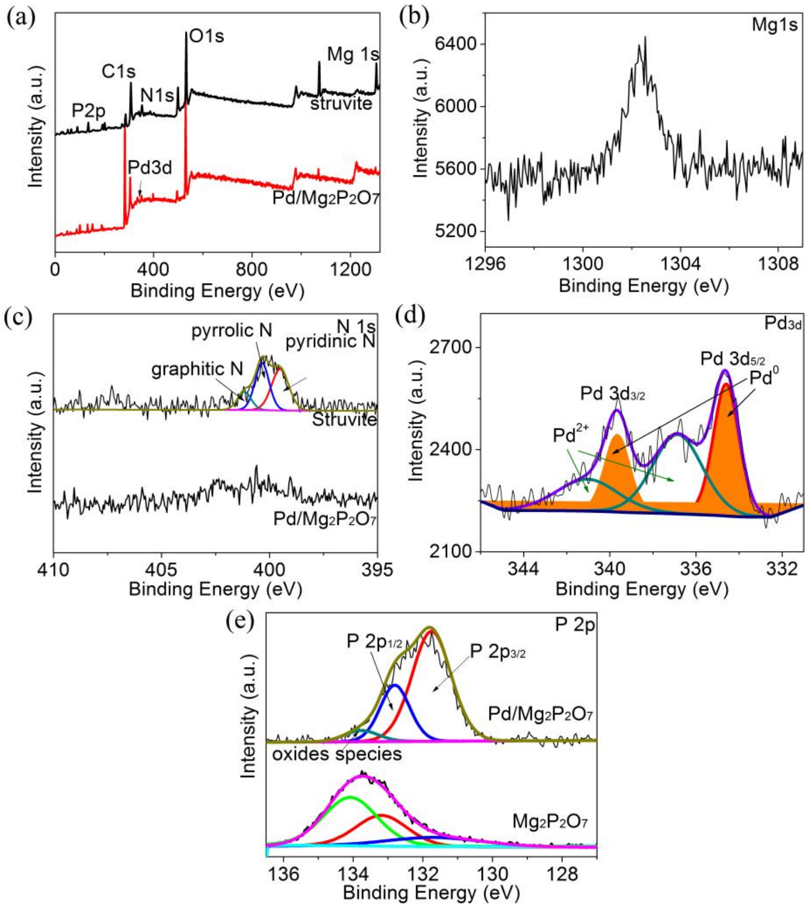

**Figure 4** (a) XPS spectra of wide-range survey, (b, c, d, e) High-resolution of the XPS profile for Mg 1s, (c) N 1s peaks, (d) Pd 3d and (e) P 2p bonds in the $Mg_2P_2O_7$ and $Pd/Mg_2P_2O_7$, respectively.

The $N_2$-adsorption/desorption measurements were conducted to study the surface area and pore-size distribution (PSD). As shown in Figure 5a, the as-synthesized struvite showed a typical adsorption-desorption behavior of type IV, which suggests the multilayers of $N_2$ were adsorbed on struvite, and interaction between the adsorbed molecules ($N_2$-$N_2$) were much stronger than that between $N_2$ and substrate ($N_2$-struvite). The specific surface area (SSA) was evaluate to be 387.6 $m^2\ g^{-1}$ by means of Brunauer-Emmett-Teller. After thermal treatment, samples of $Mg_2P_2O_7$ and $Pd/Mg_2P_2O_7$ were found to still maintain type IV adsorption behavior. The SSA of $Mg_2P_2O_7$ was 454.7 $m^2\ g^{-1}$, and the SSA of $Pd/Mg_2P_2O_7$ was 450.0

$m^2$ $g^{-1}$. To the best of our knowledge, this value of phosphate-based materials e.g., $Mg_2P_2O_7$ in terms of surface area was the largest one. This can be another evidence that struvite volatilized $NH_3$ during the heat-treatment process, and result in more mesoporous structures, thereby increased the SSA. As seen in the PSD shown in Figure 5b, the template struvite showed a relatively narrower distribution. The average pore size of struvite was about 4.1 nm, and the support $Mg_2P_2O_7$ was increased to 6.5 nm, which was due to the volatilized ammonia. The average pore size of the catalyst Pd/$Mg_2P_2O_7$ was further increased to 6.7 nm. This might be due to the fact that some small-sized Pd NPs entered into the pores during the loading process and caused partial damage to increase the average pore size. The average pore size from PSD profile obtained from Barrett-Joyner-Halenda was smaller than the TEM observation (~30 nm), and the different can be reasoned by different characterization means. The former gave an overview of the pore walls, and the later was derived from the amount of $N_2$ adsorbed in pores. As seen from TEM image (Figure 3b), the pores could be packed and cross-linked, and some of the space could not be used to accommodate $N_2$ molecules, and thus the smaller pore sized were observed. The BET specific surface areas and pore size distribution of struvite, $Mg_2P_2O_7$ and Pd/$Mg_2P_2O_7$ were listed in Table 1.

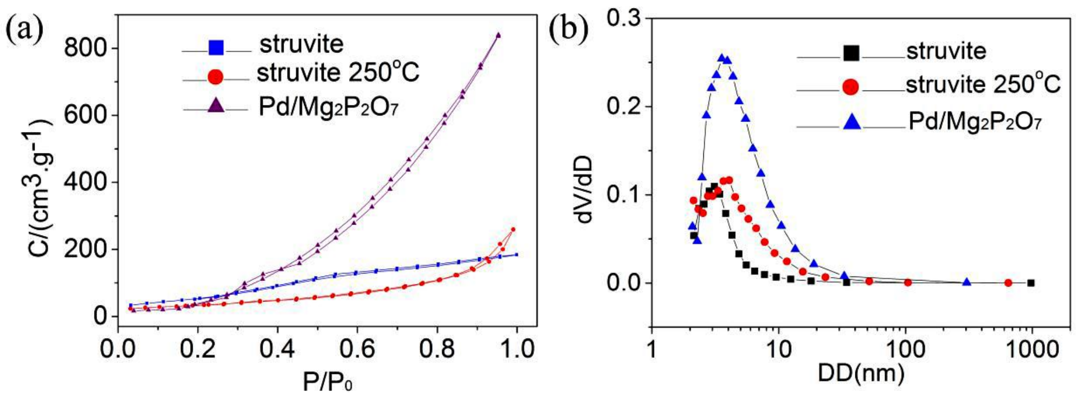

**Figure 5** (a) The $N_2$-adsorption/desorption isotherms; (b) The pore size distribution curve of the synthesized samples struvite, $Mg_2P_2O_7$ and Pd/$Mg_2P_2O_7$.

**Table 1** The specific surface area of the synthesized samples struvite, $Mg_2P_2O_7$ and $Pd/Mg_2P_2O_7$.

| Sample | Specific surface area ($m^2/g$) | Average pore size (nm) |
|---|---|---|
| struvite | 387.6 | 4.1 |
| $Mg_2P_2O_7$ | 454.7 | 6.5 |
| $Pd/Mg_2P_2O_7$ | 450.0 | 6.7 |

The FT-IR spectra of struvite, $Mg_2P_2O_7$ and $Pd/Mg_2P_2O_7$ were illustrated in Figure 6a. The broad peak at about 3428 $cm^{-1}$ was attributed to vibration of -OH [34]. The symmetry and asymmetry vibrations of N-H could also be found nearby 3428 $cm^{-1}$. The band at 1637 $cm^{-1}$ could be assigned to various antisymmetric bending of $NH_4^+$ which was the reminiscence of N-doping. By comparing the three groups in different samples, the N-H in the $Mg_2P_2O_7$-based were found to shift from 1637 to 1630 $cm^{-1}$. This shift implied that large amounts of $NH_3$ were released from the struvite. Three vibrational bands of $PO_4^{3-}$ could be found at 1079, 565 and 453 $cm^{-1}$. It is worth noting that the vibration band of Mg-O at 500 $cm^{-1}$ and the vibration of $Mg(OH)_2$ at 3700 $cm^{-1}$ were not observed in the pyrolysis sample [40]. This phenomenon demonstrated that the synthesized struvite owned high crystallinity, and most of the structure water (-OH) was removed after thermal treatment. The composite $Pd/Mg_2P_2O_7$ with addition of Pd NCs was observed to have interlayer hydrogen bonds shifted to 3430 $cm^{-1}$. To evaluate the acidity of $Pd/Mg_2P_2O_7$, the pyridine-adsorbed samples was fabricated by exposing $Pd/Mg_2P_2O_7$ to pyridine vapor, and then it was characterized by FT-IR spectrum to give qualitative analysis of acid sites [41]. The final catalyst ($Pd/Mg_2P_2O_7$) exhibited a prominent Lewis acids band at 1460 $cm^{-1}$. The band of Brönsted acids was not observed (Figure 6b). Therefore, this result proved that the catalyst was suitable to adjust electron transfer to the surface of catalyst by promoting selective adsorption of electro-withdrawing groups, e.g., nitro-aromatics, which looked forward a good performance in hydrogenation catalysis.

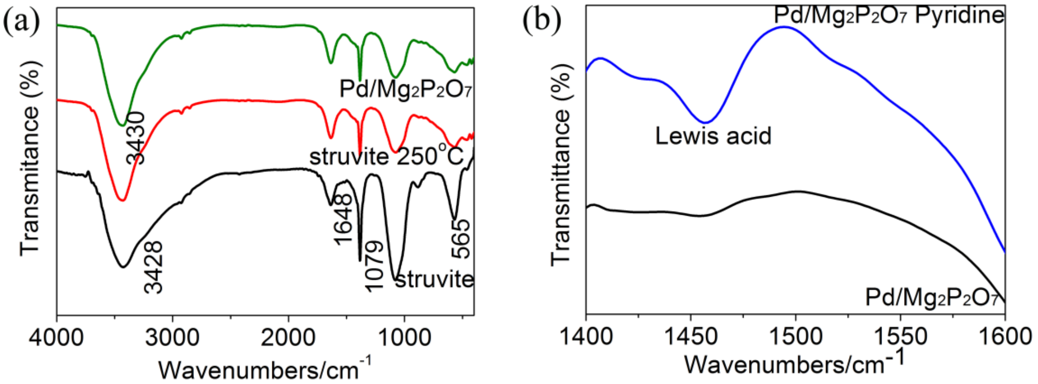

**Figure 6** (a) The FT-IR spectroscopy of the samples, (b) The FT-IR spectroscopy of pyridine adsorbed on the catalyst.

The thermogravimetry (TG) curves of struvite and Pd/struvite were given in Figure 7, which revealed the decomposition of struvite started at about 60 ℃. The major mass loss (43.2%) was found 60~120 ℃. The termination for mass loss was observed at 250 ℃, which means struvite completely transformed to Mg-pyrophosphate ($Mg_2P_2O_7$) [42]. By comparing the weightlessness curves of struvite with that of Pd/struvite, the amount of loaded Pd NPs was calculated to 3.7 wt.%. The initial incorporation of Pd was 4.0 wt.%, suggesting the strategy made full use of precious metal as heterogeneous catalysts.

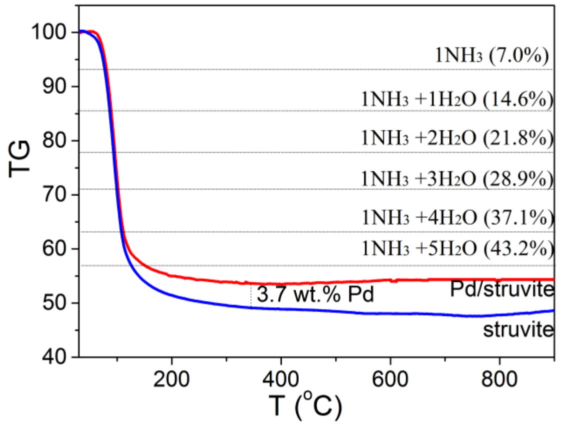

**Figure 7** The TG curves of synthesized pure struvite for a heating rate of 3 ℃/min from 25 ℃ to 900 ℃.

10.1002/chem.202100684

## 2.2 Catalysis

The catalytic performance of Pd/$Mg_2P_2O_7$ for chemoselective hydrogenation of nitrobenzene was carried out for demonstration. The nitro group is a type of strong electron-withdrawing ones which interact with electron-rich catalysts for priority [43]. The reaction was carried out at 90 ℃, 2 MPa $H_2$ and the ethanol was used as solvent. The catalytic results were listed in Table 2. The gas chromatography profiles and liquid NMR of Pd/$Mg_2P_2O_7$ selective hydrogenation of nitrobenzene were provided in the supporting information (see Figure S6&S7). In entry 1 the result was presented for bare struvite that was used in hydrogenation reaction. It could be found that the struvite had no catalytic activity. The porous $Mg_2P_2O_7$ obtained from struvite pyrolysis showed 6.3% conversion of aniline, demonstrating the Mg-pyrophosphate had little catalytic activity. Upon addition of Pd NPs, the conversion of 85.9% was observed when the nitrobenzene hydrogenation was conducted by using Pd/struvite (Entry 3), which means the Pd NPs were the active species. This indication could also be referred to the use same dosage of free Pd NPs as catalyst (Entry 4). The use of Pd/struvite only yielded a conversion of 93.1% to get aniline, while the Pd/$Mg_2P_2O_7$ showed a conversion over 99.9% within the same period (Entry 5). The catalytic performance of using $Mg_2P_2O_7$ as catalyst supports was significantly higher than struvite or free Pd NPs, which means the $Mg_2P_2O_7$ played a crucial role in the catalysis. The catalyst was synthesized from raw waste water of ChangChun as precursor with 2.0 wt.% Pd laoding which under the same synthesized condition. The catalyst also showed the high activity (entry 6). The SEM images of the struvite synthesized from raw waste water were shown in the Figure S8. The conversion of commercial catalyst (Pd/C) was also tested in this reaction to convert nitrobenzene to aniline, the conversion reached ~99.9% and the yield of aniline was 96.3% within 90 min. Another comparison experiment was carried out by using commercial Pd/$SiO_2$ as catalyst whose conversion was only 78.5% with the selectivity 92.5% (Table 2). Based on such comparisons, we came to a conclusion that interactions between Pd NPs and P in the $Mg_2P_2O_7$ played vital roles in improving the performance of hydrogenation.

The $Pd/Mg_2P_2O_7$ catalyst has the higher active for hydrogenation of nitrobenzene than varieties of reported Pd-based catalysts (Table S1).

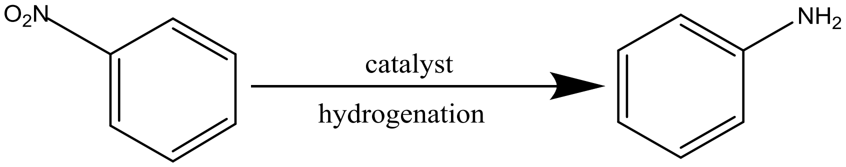

**Table 2** Hydrogenation of nitrobenzene with different samples in the work.[a]

| Entry | catalyst | Time (min) | Conversion (%) | Yield (%) |
|---|---|---|---|---|
| 1 | struvite | 60 | 3.7 | - |
| 2 | $Mg_2P_2O_7$ | 60 | 6.3 | 67.8% |
| 3 | Pd/struvite | 50 | 93.1 | 89.5% |
| 4 | $Pd/Mg_2P_2O_7$ | 50 | ＞99.9 | ＞99.0 |
| 5 | $Pd/Mg_2P_2O_7$ [b] | 50 | ＞99.9 | ＞99.0 |
| 6 | Pd/C | 90 | ＞99.9 | ＞96.3 |
| 7 | $Pd/SiO_2$ | 90 | 78.5 | 92.5% |

[a] Reaction conditions: 0.5 mmol substrate, 8.0 mL ethanol as solvent, 10.0 mg catalyst (2.0 wt.% Pd NPs loading), initial $P_{H2}$=2.0 MPa, T=90 ℃.

[b] The catalyst was synthesized from raw wastewater of Yitu ula Rever as precursor and the Pd loading was 2.0 wt.% under the same synthesis conditions as other samples.

To verify the role of the supports in the hydrogenation of nitrobenzene, the samples ($Mg_2P_2O_7$, $Pd/Mg_2P_2O_7$ and $Pd/SiO_2$) were detected by infrared spectroscopy after hydrogenation nitrobenzene at 15 min (Figure 8). Three samples contained the absorbance at 1350 and 1534 $cm^{-1}$ which are assigned to the symmetric and asymmetric stretching of the nitro group [44]. It is obvious that $Mg_2P_2O_7$ had only nitro groups on the surface. The N-H bending (1604 and 1623 $cm^{-1}$) of aniline could be found on the surface of sample $Pd/Mg_2P_2O_7$. This proves that the catalyst showed a high catalytic activity in hydrogenation at

15 min. The Pd/$SiO_2$ also showed the activation of hydrogenation nitrobenzene. However, there was an azobenzene bending at 1458cm$^{-1}$ which could be seen on the Pd/$SiO_2$ surface. This reflected that the hydrogenation process of the Pd/$SiO_2$ catalyst had complex reaction path and many by-products, thus reducing the selectivity of the target product of aniline.

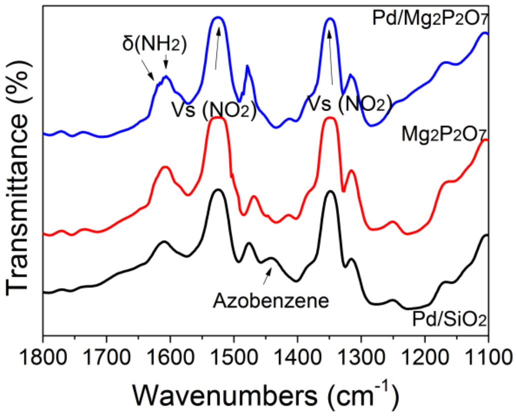

**Figure 8** The FT-IR spectra recorded at 15 min intervals during the hydrogenation of nitrobenzene adsorbed on $Mg_2P_2O_7$, Pd/$Mg_2P_2O_7$ and Pd/$SiO_2$.

Because of the high catalytic activity of the Pd/$Mg_2P_2O_7$ in the hydrogenation of nitrobenzene, the strong electronic interaction between the Pd and the support of $Mg_2P_2O_7$ acted an important role in the catalytic. Figure 9a demonstrated the loading of Pd NPs on catalytic performance under above reaction conditions (0.5 mmol substrate, 8 mL ethanol as solvent, 10 mg catalyst, initial $P_{H2}$=2.0 MPa, T=90 ℃). An increasing phenomenon in Pd NPs loading (0.5~4.0 wt.%) would improve the catalytic activity. The 2.0 wt.% Pd NPs loading catalyst could reach the nitrobenzene conversion rate at 0.572 mol g$^{-1}$ h$^{-1}$. But the Pd NPs content increased to 4.0 wt.%, the conversion rate decreased to 0.389 mol g$^{-1}$ h$^{-1}$. This might be the number of electrons in strong interactions was increased, and excessive Pd NPs would not provide electron transfer and no noticeable benefit for catalysis was obtained. The TEM, particle size distributions and XPS spectra of 4.0 wt.% Pd/$Mg_2P_2O_7$ catalyst were shown in Figure S9. The TEM image showed that the morphology of the Pd NPs is uneven, and the average particle size of Pd NPs was increased to 11.5 nm. The particle size was increased

10.1002/chem.202100684

with the loading amount. The XPS spectra of 4.0 wt.% Pd loading showed that Pd 3d did not move to the high energy banding compared to 2.0 wt.% Pd loading. So the final loading amount of Pd NPs was optimized at 2.0 wt.%. The catalytic kinetic studies of time-dependent of Pd/$Mg_2P_2O_7$ for hydrogenation of nitrobenzene were shown in Figure 9b. It was found that the conversion of nitrobenzene reached >99.0% at 50 min, and the selectivity of aniline was 99.0%.

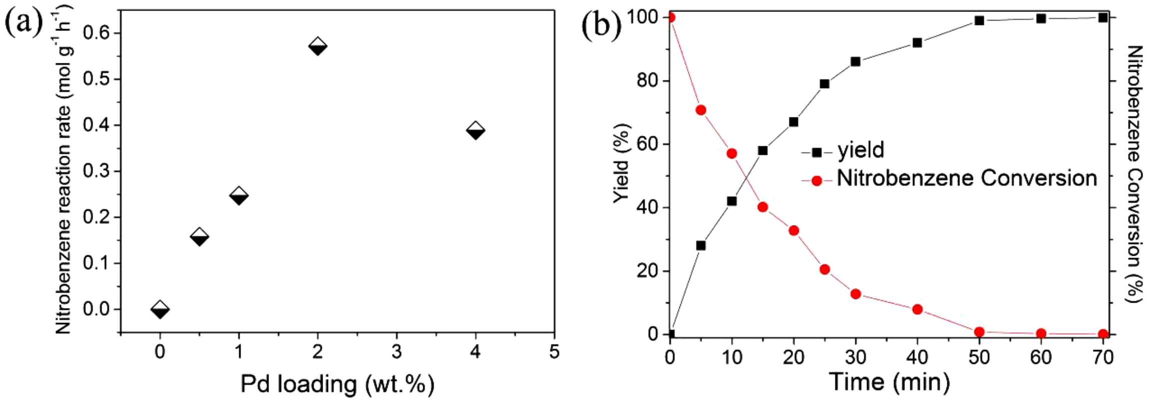

**Figure 9** (a) Effect Pd NPs loading on the hydrogenation reaction rate; (b) The catalytic kinetic studies of time-dependent of Pd/$Mg_2P_2O_7$ for hydrogenation of nitrobenzene.

The effect of different solvents on the chemoselective hydrogenation of nitrobenzene was also further investigated (Figure 10). By using ethanol as solvent, the yield of aniline was obtained at 99.9% with the reaction time of 50 min. Although the yield of reached to 99.0% with water as solvent, the reaction time was 60 min. The other three solvents (THF, DMF and cyclohexane) showed unsatisfied yield of aniline throughout the reaction, the yields were 28.2%, 63.7% and 76.1% at 60 min of catalytic reaction, respectively. Industrial catalysis often requires consideration of reaction rate. Hence the optimized solvent was selected the ethanol.

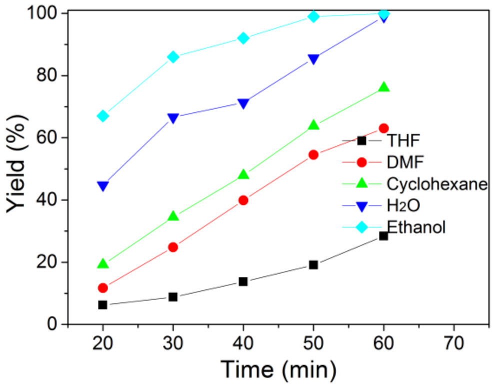

**Figure 10** The effect of different solvents on the chemoselective hydrogenation of nitrobenzene.

The activity of $Pd/Mg_2P_2O_7$ was also evaluated in hydrogenation of other derivatives of nitrobenzene. The halogenated nitrobenzenes were tested for selective hydrogenation to corresponding halogenated anilines (Table 3). The catalyst $Pd/Mg_2P_2O_7$ showed conversion over 99.0% within 60 min (entries 1-5). The selectivity to the halogenated anilines was about 80.0% due to the dehalogenation [45, 46]. Under similar conditions, the catalytic hydrogenation of nitroaniline (entry 6) exhibited a conversion of 99.0%, and the selectivity was about 99.0%. The 4-nitrophenol (nitroarenes with -OH, entry 7) also showed conversion and selectivity over 99.0% within 90 min. These results confirmed the general applicability of our prepared $Pd/Mg_2P_2O_7$ for selective hydrogenation of nitro compounds.

**Table 3** The conversion and selectivity for hydrogenation catalysis on various nitroarenes using our prepared $Pd/Mg_2P_2O_7$. [a]

| Entry | Substrate | Product | Time (min) | Conversion (%) | Selectivity (%) |
|---|---|---|---|---|---|
| 1 | 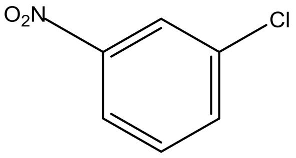 | 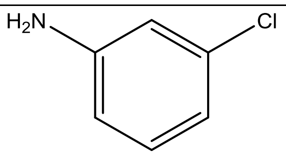 | 60 | ＞99.0 | 81.8 |

| | | | | | |
|---|---|---|---|---|---|
| 2 | 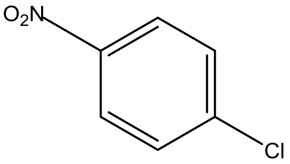 | 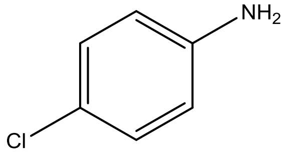 | 60 | ＞99.0 | 76.3 |
| 3 | 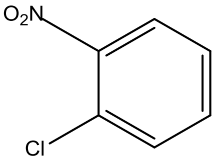 | 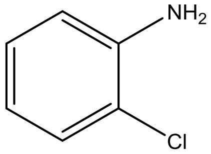 | 60 | ＞99.0 | 84.6 |
| 4 | 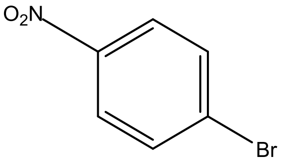 | 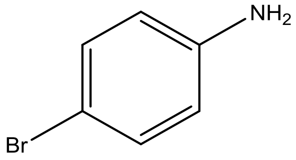 | 60 | ＞99.0 | 89.7 |
| 5 | 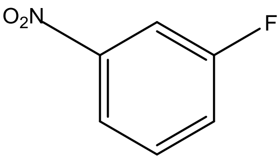 | 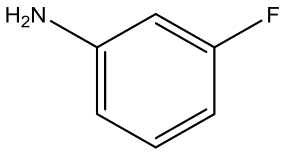 | 60 | ＞99.0 | 77.6 |
| 6 | 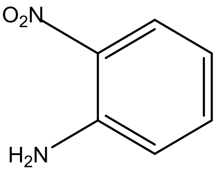 | 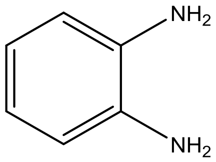 | 90 | ＞99.0 | ＞99.0 |
| 7 | 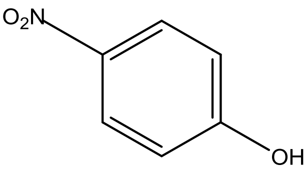 | 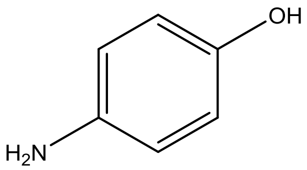 | 90 | ＞99.0 | ＞99.0 |

[a] Reaction conditions: 0.5 mmol nitroarene with ethanol as solvent, 10 mg catalyst of $Pd/Mg_2P_2O_7$, $P_{H2}$=2.0 MPa and 90 ℃.

The $Pd/Mg_2P_2O_7$ exhibited a high stability with no obvious deactivation when the material was reused for 5 cycles (Figure 11). The hydrogenation reaction of nitrobenzene was selected as a representative one. In cycling experiments of the nitrobenzene hydrogenation, the conversion was found to have no decreasing of activity, and remained 99.0% after 5 runs of tests. To detect the loss of Pd NPs during the repeated tests, the ICP-AES was measured, and results showed that the loss of Pd was less than 0.7%. The TEM of $Pd/Mg_2P_2O_5$ catalyst after

10.1002/chem.202100684

reused 5 times for nitrobenzene hydrogenation to aniline was also shown in Figure S10. Nitro group is a strong electron withdrawing group, and the surface of catalyst needs to have sufficient electrons when designing the catalyst. The support of $Mg_2P_2O_7$ has a large number of oxygen vacancy which offers strong Lewis sites [47, 48]. The oxygen vacancies in crystal structure of struvite and $Mg_2P_2O_7$ were schemed in Figure 12. These oxygen vacancies would accelerate the electron transfer, i.e., electrons of Pd NPs transferred to the $Mg_2P_2O_7$, so the surface of catalyst was enriched with sufficient electrons to convert nitro groups, and the N and P provided the metal-like electronic structure generating more defect sites.

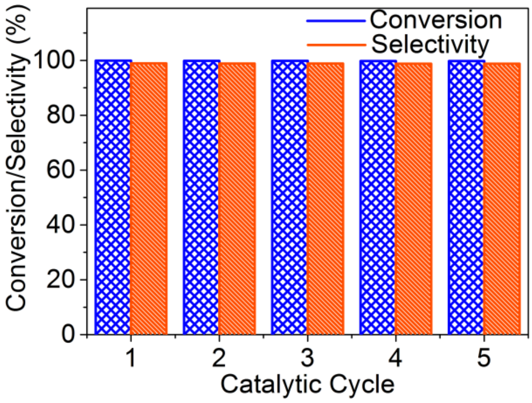

**Figure 11** Reuse of the $Pd/Mg_2P_2O_7$ for chemoselective hydrogenation of nitrobenzene in which the reactions conditions were conducted under conditions: T=90 ℃, $P_{H2}$=2.0 MPa, and reaction time=50 min.

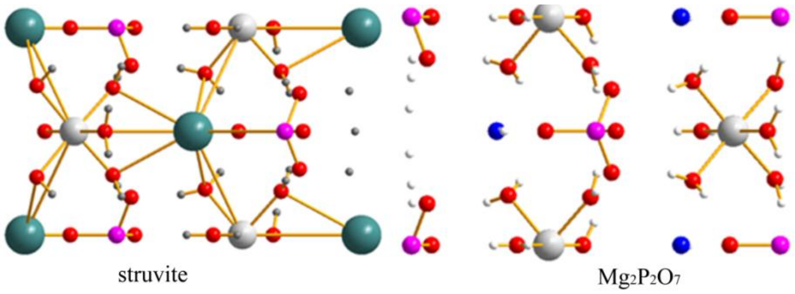

**Figure 12** Oxygen vacancies in the crystal structure of struvite and $Mg_2P_2O_7$.

## 3. Conclusions

In conclusion, a type of fibrous catalyst Pd/$Mg_2P_2O_7$ had been successfully prepared by using struvite as template that was synthesized from wastewater. The composite Pd/$Mg_2P_2O_7$ was demonstrated to have unprecedented specific surface areas (450.0 $m^2$ $g^{-1}$) among the type of Mg-phorsphate materials. The high activity on chemoselectivity hydrogenation of nitro-aromatics including nitrobenzene and its derivatives was demonstrated, and the yield of target anilines was >75% at a conversion of ~99%. The halogen-free nitro substrates were found to have a high conversion of ~99.0% as well as the high selectivity of ~99.0%. The prepared Pd/$Mg_2P_2O_7$ catalyst was able to be reused at least five times, and to the activity and selectivity for hydrogenation of nitroarenes were remained. This strategy provided a new pathway in preparing highly efficient catalysts as well as gave a solution to alleviate eutrophication pollution consisting with N and P-containing substances.

## Experimental sections

### Chemicals

Chemicals used in this research were provided by Aladdin-E.Com which includes magnesium chloride hexahydrate ($MgCl_2$ $6H_2O$), ammonium chloride ($NH_4Cl$), sodium chloride (NaCl), ammoniumphosphate ($(NH_4)_2HPO_4$), sodium hydroxide (NaOH), sodium tetrachloropalladate ($Na_2PdCl_4$), potassium chloride (KCl), potassium bromide (KBr), ascorbic acid (short for ‘AA’), polyvinylpyrrolidone (58000, K29-32, short for ‘PVP’), nitrobenzene, aniline, 1-Chloro-4-nitrobenzene, 4-Chloroaniline, o-Chloronitrobenzene, 2-Chloroaniline, 1-Chloro-3-nitrobenzene, m-Chloroaniline, 1-Bromo-4-nitrobenzene, 4-Bromoaniline, 3-Fluoronitrobenzene, 3-Fluoroaniline, 2-Nitroaniline, o-Phenylenediamine, p-Nitrophenol and 4-Aminophenol. All the above chemicals were of analytical purity and were used without further purification.

**Synthesis of struvite nano-fibers**

The synthetic experiments were carried out at room temperature. The simulated wastewater was prepared at a molar ratio of 1:1:3 for $Mg^{2+}$:$PO_4^{3-}$:$NH_4^+$ [33]. Typically, 0.0407 g of $MgCl_2$ $6H_2O$ was dissolved in 40 mL of deionized water under stirring for 5 min (solution A). The amount of 0.0264 g of $(NH_4)_2HPO_4$ and 0.0107 g of $NH_4Cl$ were added in 10 mL of deionized water under magnetic stirring for 5 min to obtain solution B. The two kinds of solution (A&B) were mixed, and was homogenized using ultrasound for 10 min. The next step was precipitation of struvite by adding NaCl (3.5 wt.%) to the above mixed solution, and the pH of the solution was adjusted at pH=11 using 0.2 mol/L NaOH aqueous solution. Afterward the solution was stirred at 800 rpm for 12 hrs on a magnetic stirrer. The product was reclaimed via centrifugation (9000 rpm for 5 min) and washed with ethanol several times. Finally, the obtained struvite was dried in vacuum at room temperature for overnight.

**Loading Pd NPs on mesoporous $Mg_2P_2O_7$**

To prepare mesoporous materials, the as-synthesis struvite powders (proven to be $Mg_2P_2O_7$ nano-fibers) were decomposed at the temperature of around 250 ℃ with different pyrolysis rates. The Pd nanoparticles (NPs) were synthesized according to the previous method [49]. To load Pd NPs on the mesoporous $Mg_2P_2O_7$, the 0.5, 1.0, 2.0 and 4.0 wt.% Pd NPs gel (dispersed in methanol) was added into the above $Mg_2P_2O_7$ in methanol with stirring under reflux for 1 h. The material was reclaimed by centrifugation followed by drying at 105 ℃ overnight.

**Material characterizations**

The X-ray diffraction (XRD) was performed on a Regaku D/max-5000 operating at 40 kV and 20 mA equipped with Cu Kα radiation. Data were recorded within the 2θ of 5-80 ° at the speed of 0.05 °/20 s per step. The morphology was examined by scanning electron microscope (FE-SEM, Hitachi SU8020). The transmission electron microscope (HRTEM, JEOL JEM-2100F) with an accelerating voltage of 200 kV was used to examine the microstructure. The thermal behavior was investigated by using the thermogravimetric analysis (TG, Netzsch), and the measurement were recorded in $N_2$ atmosphere at the heating steps of 5 ℃/min from 25 ℃ to 1000 ℃. The specific surface area (SSA) and pore-size distribution (BJH) were measured on a Micromeritics Tristar II 3020M ($N_2$ adsorption-desorption). The X-ray photoelectron spectroscopy (XPS) was recorded on an ESCALAB MK II spectrometer and the Mg-Ka X-ray line (1253.6 eV) was used as the excitation source. The accurate binding energy was determined with respect to the position of C 1s peak at 284.8 eV as the reference. Fourier transform infrared spectrum (FT-IR) measurements were collected on a Nicolet 6700 spectrometer, with wavenumber ranging from 4000 and 400 $cm^{-1}$. To estimate the work functions of the catalysts, the data was obtained using a scanning Kelvin probe system SKP5005 (KP Technology Ltd.). $\Phi=E_V-E_F$, where $\Phi$ is work function, $E_V$ and $E_F$ were represented the vacuum level and Fermi level. The Pd and N concentration of the digested solution (using 1.0 M $HNO_3$) from samples used in this experiment was detected by inductively coupled plasma atomic emission spectroscopy (ICP-AES).

**Catalyst performance test**

The catalytic performance on hydrogenation of nitroarenes was evaluated on a 50 mL stainless vessel equipped with magnetic stirring and heating unit with adjustable hydrogen pressure. For a typical catalytic reaction 0.50 mmol nitroarenes and 10.0 mg catalyst were mixed in 8.0 mL ethanol. The reaction was implemented in the vessel. The reactor was purged with $H_2$ for three times to replace the air. Then the device was heated up to the target reaction temperature within 10 min, and charged with 2.0 MPa of hydrogen at 90 ℃. After reaction, the stainless vessel was cooled down to room temperature. Samples were centrifugalized and analyzed by gas chromatography mass spectrometry systems (GC-MS) using n-heptane as internal standard.

**Acknowledgements**

We acknowledged financial supports by National Natural Science Foundation of China (51874145), the guide project of Jilin Science and technology development plan in 2020 (20200401028GX), China Ocean Mineral Resources R&D Association (COMRA) Special Foundation (DY135-46, DY135-R2-1-01), and the Province/Jilin University co-construction project – funds for new materials – (SXGJSF2017-3).

## References

[1] Z. X. Tan, A. Lagerkvist, *Renew. Sust. Energ. Rev.* **2011**, *15*, 3588-3602.

[2] A. Bouzas, N. Marti, S. Grau, R. Barat, D. Mangin, L. Pastor, *J. Cleaner Prod.* **2019**, *227*, 130-140.

[3] H. Li, Q. Z. Yao, Z. M. Dong, T. L. Zhao, G. T. Zhou, S. Q. Fu, *ACS Sustainable Chem. Eng.* **2018**, *7*, 2035-2043.

[4] X. Liu, J. Wang, *Chem. Eng. J.* **2019**, *378*.

[5] T. Zhang, L. Ding, H. Ren, X. Xiong, *Water Res*. **2009**, *43*, 5209-5215.

[6] J. D. Doyle, S. A. Parsons, *Water Res.* **2002**, *36*, 3925-3940.

[7] Y. Luo, H. Li, Y. R. Huang, T. L. Zhao, Q. Z. Yao, S. Q. Fu, G. T. Zhou, *Chem. Eng. J.* **2018**, *351*, 195-202.

[8] H. D. Ryu, D. Kim, S. I. Lee, *J. Hazard. Mater.* **2008**, *156*, 163-169.

[9] J. F. Hartwig, *Nature* **2008**, *455*, 314-322.

[10] M. Orlandi, D. Brenna, R. Harms, S. Jost, M. Benaglia, *Org. Process Res. Dev.* **2018**, *22*, 430-445.

[11] S. Y. Nie, S. Z. Yang, P. F. Zhang, *Chem. Eng. Sci.* **2020**, *220*, 115619.

[12] S. Xue, A. Chai, Z. Cai, Y. Wei, C. Xiang, W. Bian, J. Shen, *Dalton Trans.* **2008**, 4770-4775.

[13] L. Chen, Z. Gao, Y. Li, *Catal. Today* **2015**, *245*, 122-128.

[14] Y. Shu, H. Chen, N. Q. Chen, X. L. Duan, P. F. Zhang, S. Z. Yang, Z. H. Bao, Z. L. Wu,

S. Dai, *Chem* **2020**, *6*, 1723-1741.

[15] S. J. Tauster, S. C. Fung, R. L. Garten, *J. Am. Chem. Soc.* **1978**, *100*, 170-175.

[16] P. A. Khomyakov, G. Giovannetti, P. C. Rusu, G. Brocks, J. van den Brink, P. J. Kelly, *Phys. Rev. B* **2009**, *79*.

[17] H. Zhang, C. Zhang, Y. Zhang, P. Cul, Y. Zhang, L. Wang, H. Wang, Y. Gao, *Appl. Surf. Sci.* **2019**, *487*, 616-624.

[18] Y. He, W. T. Sun, S. C. Wang, P. A. S. Reed, F. C. Walsh, *Electrochim. Acta* **2017**, *245*, 872-882.

[19] Y. Zhang, J. J. Wang, J. W. Ren, X. H. Liu, X. C. Li, Y. J. Xia, G. Z. Lu, Y. Q. Wang, *Catal. Sci. Technol.* **2012**, *2*, 2485-2491.

[20] J. H. Zhao, Y. Shu, P. Z. Zhang, *Chin. J. Catal.* **2019**,*40*,1078.

[21] R. H. Lin, Y. J. Ding, *Materials* **2013**, *6*, 217-243.

[22] N. Ma, A. A. Rouff, B. L. Phillips, *ACS Sustainable Chem. Eng.* **2014**, *2*, 816-822.

[23] Z. L. Li, J. H. Liu, C. G. Xia, F. W. Li, *ACS Catal.* **2013**, *3*, 2440-2448.

[24] M. Vanni, M. Serrano-Ruiz, F. Telesio, S. Heun, M. Banchelli, P. Matteini, A. M. Mio, G. Nicotra, C. Spinella, S. Caporali, A. Giaccherini, F. D'Acapito, M. Caporali, M. Peruzzini, *Chem. Mater.* **2019**, *31*, 5075-5080.

[25] H. Li, W. Shan, S. Shen, Y. Ren, D. Zhang, R. Sun, Z. Zhou, X. Ma, *J. Cleaner Prod.* **2019**, *228*, 965-973.

[26] S. Tahmasebi, J. Mokhtari, M. R. Naimi-Jamal, A. Khosravi, L. Panahi, *J. Organomet. Chem.* **2017**, *853*, 35-41.

[27] P. Serna, A. Corma, *ACS Catal.* **2015**, *5*, 7114-7121.

[28] R. Ueyama, N. Seki, T. Ueyama, K. Koumoto, K. Kuribayashi, *J. Ceram. Soc. Jpn.* 108 **2000**, *108*, 661-665.

[29] H. Li, Q. Z. Yao, Z. M. Dong, T. L. Zhao, G. T. Zhou, S. Q. Fu, *ACS Sustainable Chem. Eng.* **2019**, *7*, 2035-2043.

[30] Y. Sun, B. Huang, N. Xu, Y. Li, M. Luo, C. Li, Y. Qin, L. Wang, S. Guo, *Sci. Bull.* **2019**, *64*, 54-62.

[31] Z. Y. Li, J. F. Li, K. H. Jiang, S. Y. Yuan, D. K. Yu, H. Wei, Z. M. Shi, X. T. Li, H. B. Chu, *Chem. Eng. J.* **2021**, *411*, 128527.

[32] Y. Z. Li, L. Xu, B. Xu, Z. P. Mao, H. Xu, Y. Zhong, L. P. Zhang, B. J. Wang, X. F. Sui, *ACS Appl. Mater. Interfaces* **2017**, *9*, 17156-17163.

[33] J. Silvestre-Albero, G. Rupprechter, H. J. Freund, *Chem. Commun.* **2006**, 80-82.

[34] L. Wei, T. Hong, X. Li, M. Li, Q. Zhang, T. Chen, *Chem. Eng. J.* **2019**, *358*, 1074-1082.

[35] J. Shan, X. Sun, S. Zheng, T. Wang, X. Zhang, G. Li, *Carbon* **2019**, *146*, 60-69.

[36] Y. Zhu, F. Wang, M. Fan, Q. Zhu, Z. Dong, *J. Colloid Interface Sci*. **2019**, *553*, 588-597.

[37] M. Caporali, A. Guerriero, A. Ienco, S. Caporali, M. Peruzzini, L. Gonsalvi, *Chemcatchem* **2013**, *5*, 2517-2526.

[38] Z. X. Su, R. Pang, X. Y. Ren, S. F. Li, *J. Mater. Chem. A* **2020**, *8*,17238.

[39] A. Krittayavathananon, P. Iamprasertkun, M. Sawangphruk, *Carbon* **2016**, *109*, 314-320.

[40] Y. Cai, C. Li, D. Wu, W. Wang, F. Tan, X. Wang, P. K. Wong, X. Qiao, *Chem. Eng. J.* **2017**, *312*, 158-166.

[41] P. Zhang, F. J. Zhu, X. L. Tan, W. Q. Li, S. N. Xu, P. P. Zhang, C. D. Wei, S. D. Miao, *Appl. Clay Sci.* **2018**, *166*, 207-213.

[42] J. Hoevelmann, T. M. Stawski, R. Besselink, H. M. Freeman, K. M. Dietmann, S. Mayanna, B. R. Pauw, L. G. Benning, *Nanoscale* **2019**, *11*, 6939-6951.

[43] X. J. Yang, B. Chen, L. Q. Zheng, L. Z. Wu, C. H. Tung, *Green Chem.* **2014**, *16*, 1082-1086.

[44] G. Richner, J. A. V. Bokhoven, Y. M. Neuhold, M. Makosch, K. Hungerbuhler, *Phys. Chem. Chem. Phys.* **2011**, *13*, 12463-12471.

[45] X. L. Cui, H. Li, M. Yuan, J. Yang, D. Xu, Z. Y. Li, G. Q. Yu, Y. M. Hou, Z. P. Dong, *J. Colloid Interf. Sci.* **2017**, *506*, 524-531.

[46] V. Nagpal, A. D. Bokare, R. C. Chikate, C. V. Rode, K. M. Paknikar, *J. Hazard. Mater.* **2010**, *175*, 1-3.

[47] J. Y. Luo, L. J. Chen, Y. J. Zhao, P. He, Y. Y. Xia, *J. Power Sources* **2009**, *194*, 1075-1080.

[48] Y. Shu, J. F. Bao, S. Z. Yang, X. L. Duan, P. F. Zhang, *AIChE J.* **2021**, *67*,e17046.

[49] P. Zhang, Z. Y. Wang, Y. Zhang, J. Wang, W. Q. Li, L. N. Li, P. P. Zhang, C. D. Wei, S. D. Miao, *Appl. Catal. a-Gen.* **2020**, *597*, 117540.

10.1002/chem.202100684

Text for TOC:

A novel strategy was provided to synthesize fibrous struvite from wastewater, and an ultrahigh surface area composite Pd/$Mg_2P_2O_7$ with mesopous structure was fabricated via template way. The prepared Pd/$Mg_2P_2O_7$ nanowires showed brilliant performance in selective hydrogenation of nitrobenzenes. This strategy provided a new pathway in synthesizing highly efficient catalysts as well as gave a solution to alleviate eutrophication pollution consisting with N and P-containing substances in wastewater.

**TOC Figure:**